Quasibound states in a one-dimensional grating for electro-optic modulation

Zhuang Li, Xiaotian Zhang, Zhenshan Zhai, Yangjian Cai, and Xianyu Ao *

Shandong Provincial Engineering and Technical Center of Light Manipulation and Shandong Provincial Key Laboratory of Optics and Photonic Devices, School of Physics and Electronics, Shandong Normal University, Jinan 250358, China

(Received 18 June 2022; accepted 24 August 2022; published 1 September 2022)

For modulation in free space using the linear electro-optic effect, a narrow-linewidth resonance is favorable when a minimal voltage is preferred to fully shift the resonance. Here a method is proposed to engineer the quasibound states in a slab waveguide consisting of electro-optic polymer and metal gratings, in order to achieve narrow-linewidth resonances for electro-optic modulation. This quasibound state features a strong out-of-plane electric field component located at the position of the metal strips constituting the grating, which also work as the interdigitated electrodes, and thus, the optical mode can interact with the electrostatic field efficiently. The radiation damping of the quasibound state can be controlled by changing the relative position of the neighboring metal strips, while the optical mode can maintain the same periodicity as the electrostatic field. This method also offers prospects for engineering narrow-linewidth resonances for other applications.

DOI: 10.1103/PhysRevB.106.125101

I. INTRODUCTION

Pixelized flat optical components that can locally change the amplitude, phase, or polarization of transmitted or reflected light in free space, if being actively tuned, can find applications in spatial light modulators and free-space optical communications [1]. Many active materials and device architectures have been exploited in order to achieve high operating speed when driven via electrical actuation, for example, by modulating the second-order nonlinearity in a Kretschmann configuration [2], free carrier in transparent conducting oxides [3–6], and quantum-confined Stark effect in semiconducting structures [7]. On the other hand, guided wave integrated modulators utilizing the linear Pockels effect can operate at bandwidths well exceeding tens of gigahertz [8,9]. In a Pockels electro-optic (EO) switch or modulator, the refractive index of the EO materials is changed in response to an externally applied voltage. Compared to traditional inorganic EO materials, polymers with much higher EO coefficients have been developed recently [10]. For an EO polymer, an efficient poling mechanism and effective device layout are also required to achieve large EO effects, through reaching a large EO coefficient r_{33} from the poling process and maximizing the overlap integral factor between the electrostatic and optical fields.

Recently, one-dimensional metal gratings have attracted great interest in the study of EO polymer-based modulators [11–15] when considering free-space coupling with light beams impinging upon the device along the surface normal direction. The metal gratings can induce plasmonic resonances around which transmission or reflection changes dramatically, and at the same time, can serve as the electrodes for applying the poling and driving voltage. There are basically two types of device layout with metal gratings. In the vertical metal-polymer-metal layout [11–14], the whole metal grating serves as one electrode, while another conductive plane serves as the counterelectrode. In this way, the EO polymer is poled along the out-of-plane direction. However, the properties of the EO polymer may be degraded during the fabrication of the metal grating on top [11,12]. In the other layout, the metal grating is patterned on a substrate and the EO polymer is then coated on top [16]. The EO polymer has a higher refractive index than air above and the substrate below to form a slab waveguide. The metal strips constituting the grating can serve as interdigitated electrodes. The fields for polling and modulating can be considered the same under the electrostatic approximation, and the second-order susceptibility is a vector field following the applied electrostatic fields.

In the waveguide-grating hybrid system, guided mode resonances [17] can be formed through the interaction between the slab waveguide and the metal grating. The optical intensity inside the EO polymer layer can then be much higher than that of the incident beam, and the modulation of the incident beam can be enhanced accordingly. Narrow-linewidth resonances are favorable when a minimal voltage is preferred to fully shift the resonance. To this end, resonances evolved from bound states in the continuum (BICs), called quasi-BICs, can reach a very narrow linewidth. BICs are a nonradiating eigenmode of an open system, theoretically exhibiting an infinite quality (Q) factor in lossless systems. As hybrid plasmonic-photonic systems, the two types of device layout mentioned above can support symmetry-protected and Friedrich-Wintgen BICs [18–22]. EO modulation utilizing quasi-BIC modes has been demonstrated in Ref. [23], based on two-dimensional periodic arrays of in-plane asymmetric silicon nanostructures covered with the EO polymer. However, additional metal interdigitated electrodes placed in between the silicon units for applying the poling and driving voltage should be defined after the fabrication of silicon nanostructures, making the fabrication process very complicated.

*aox@sdnu.edu.cn

 ©2022 American Physical Society

In this work, we propose a hybrid system consisting of a one-dimensional metal grating and slab waveguide, where the guided mode resonance and the electrostatic field have the same periodicity, in order to promote the overlap factor and induce narrow-linewidth resonances simultaneously. We start from a bound mode, which is at the edge of the irreducible Brillouin zone and below the light line. This mode possesses a strong out-of-plane electric field component located at the position of the metal strips and thus can efficiently interact with the electrostatic field. To make this mode accessible from free space, we perturb the system by slightly changing the relative position of the neighboring metal strips to turn this mode weakly bright, whereas the characteristics of the mode distribution for the unmodified system can be well maintained. The quality factor of the modified system ($Q \approx 3000$) is very close to that of the unmodified system, because it is limited by the dissipative losses in the metal. We estimate that the required driving voltage to fully shift the resonance can be well below 10 V. We verify the above narrow-linewidth resonances experimentally using alumina to mimic the EO polymer.

II. HYBRID SYSTEM CONSISTING OF GOLD GRATING AND EO POLYMER SLAB WAVEGUIDE

Figure 1(a) depicts the proposed device layout for EO modulation, consisting of a one-dimensional gold grating placed in between a silica substrate and an EO polymer layer. The EO polymer has a higher refractive index than the silica substrate and thus both guided modes and guided mode resonances can exist. The external voltage can be applied by using the metal strips of the grating as interdigitated electrodes. In Fig. 1(b) we show the electrostatic field with a constant voltage V_0 applied to the interdigitated electrodes. The electrostatic field from one biased metal strip is directed in opposite directions toward the ground electrodes on the two sides. As explained in Ref. [16], the EO polymer in the adjacent units of the array are poled in opposite directions, yielding alternating EO coefficients r_{33} and $-r_{33}$, and consequently, the neighboring units experience the same refractive index change (instead of canceling each other) upon an applied driving voltage.

We begin by considering a one-dimensional system with gold strips of equal width ($w_1 = w_2 = 150$ nm) and equal distance in between ($d_1 = d_2 = 500$ nm). These parameters should be technically feasible, since aluminum gratings with a similar period and strip width have been used as interdigitated electrodes for liquid crystals previously [24,25]. Numerical simulations were carried out using a commercial finite-element solver (COMSOL), by setting up a unit cell with a *pseudo*period $\Lambda = d_1 + d_2$ and surrounded with absorbing boundary conditions on the top and bottom surfaces of the computational domain. For the polymer layer we assumed the optical constants to be the EO polymer (JRD1:PMMA) in Ref. [16], and for the silica substrate the refractive index was assumed to be $n = 1.44$. The dielectric function of gold was obtained from Johnson and Christy [26]. The thickness of the metal strips and of the polymer layer is $h = 50$ nm and $t = 500$ nm, respectively. We focus on the polarization for which the electric field stays inside the xz plane (TM polarization). Around the wavelength $\lambda = 1500$ nm, this system supports two eigenmodes which cannot be excited by external plane waves [Figs. 1(c) and 1(d)]. The electric field forms two curls of opposite directions within the pseudo-unit-cell, where

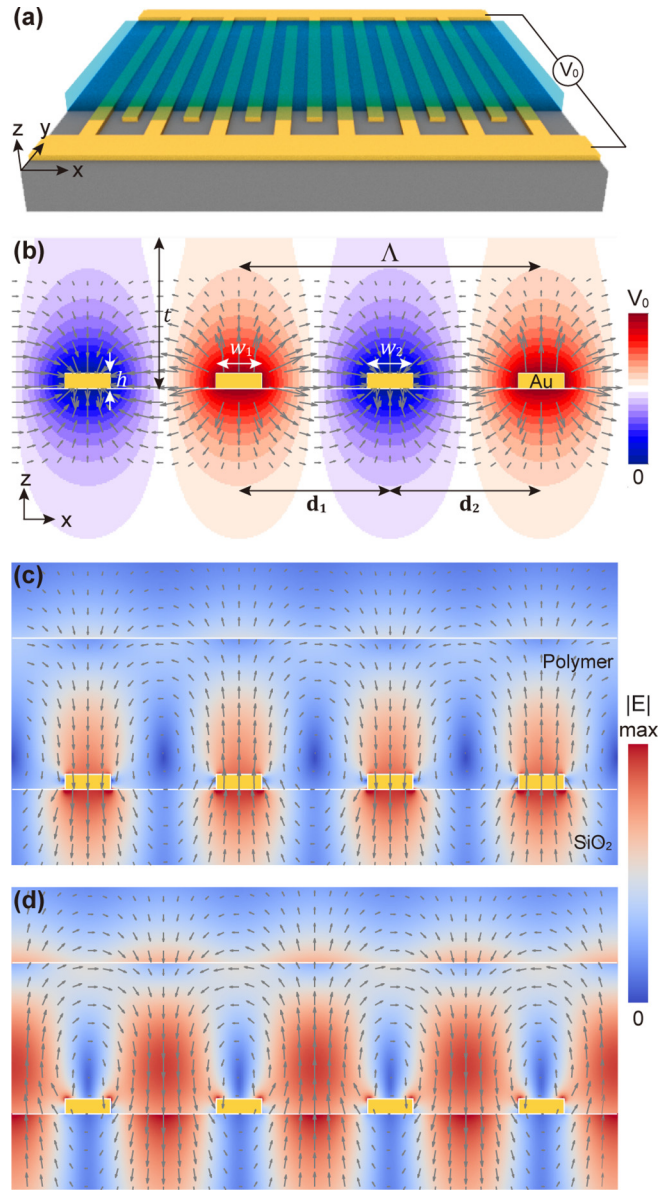

FIG. 1. (a) Schematic of the proposed device for modulation. A one-dimensional gold grating, which also serves as the interdigitated electrodes, is deposited on the quartz substrate, and finally covered with a film of electro-optic polymer. One set of the electrodes is connected to the ground while the other set is at the potential V_0. (b) Cross section showing electrostatic field. The color indicates the amplitude of the electric potential, while the gray arrows indicate the direction of the electrostatic field. (c), (d) Dark modes supported by the one-dimensional system with a pseudoperiod $\Lambda = d_1 + d_2 = 2d_1 = 2d_2 = 1000$ nm, metal width $w_1 = w_2 = 150$ nm, metal thickness $h = 50$ nm, and polymer film thickness $t = 500$ nm. The color indicates the amplitude of the electric field, while the gray arrows indicate the direction of the electric field at optical frequency. Inside the polymer layer, the distribution of the optical mode in (c) matches with the distribution of the static electric field in (b).

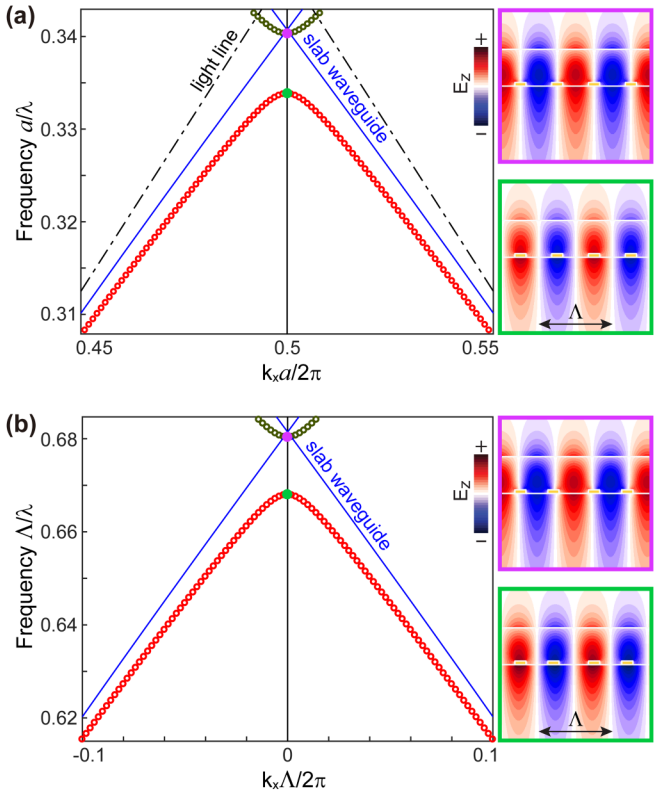

FIG. 2. Band diagram of a slab with one-dimensional periodicity along the x axis, with (a) period $= \Lambda/2 = a$, and (b) period $= \Lambda$ and $|d_1 - d_2|/2 = 50$ nm. Other parameters are the same as in Fig. 1. Black dash-dotted lines are the light lines of the silica substrate. Blue solid lines are the lowest-order mode of the slab without the metal grating, and open circles are the modes with the presence of the grating. Only modes with electric field inside the xz plane are considered. The mode profiles of the E_z component at the band edges are shown on the right.

the z component experiences the largest enhancement. The enhanced electric field is located at the position of the metal strips in Fig. 1(c), while in Fig. 1(d) the enhanced electric field is in between the metal strips.

Because the optical fields in Fig. 1(c) and Fig. 1(d) alternate in direction at each site of the metal strips, they can be regarded as the band-edge modes at the X point of the irreducible Brillouin zone of a one-dimensional system with period $a = \Lambda/2$ [Fig. 2(a)]. The lowest-order guided mode of the slab without the metal grating is shown as the blue solid lines. With the presence of the metal grating (open circles), a band gap opens, and the modes below the light line are guided modes [27], despite the fact that dissipative losses exist in the metal and EO polymer. For $k_x = \pi/a$, the modes have a wavelength of $2a$ and form standing waves. The electric field associated with the lower band-edge mode is strongly concentrated in the metal regions, while the upper one has its electric field in between the metal strips in order to be orthogonal to the lower one, just like what are shown in Figs. 1(c) and 1(d).

In order to make these modes accessible by external plane waves, we then lower the symmetry of the above one-dimensional system by making the metal strips of the

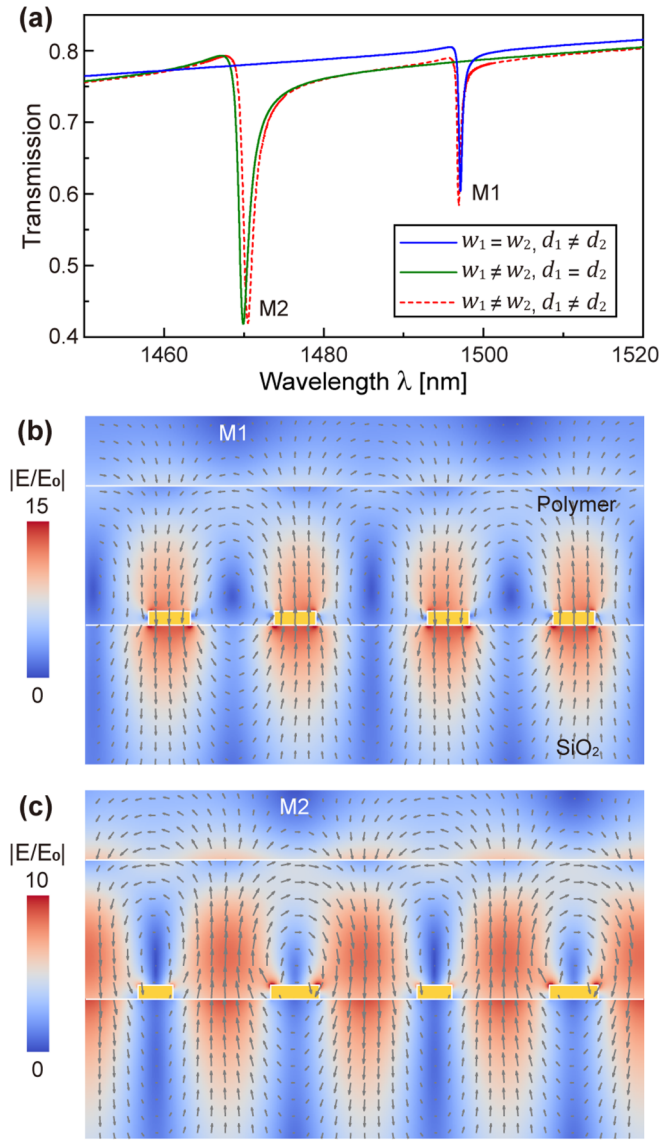

FIG. 3. Resonances induced by either nonequal distance or nonequal width in metal strips. (a) Transmission spectra under x-polarized plane-wave excitation at normal incidence for either nonequal distance ($|d_1 - d_2|/2 = 50$ nm) or nonequal width ($|w_1 - w_2|/2 = 50$ nm). The spectra with both changes together are also shown for reference. Other parameters are fixed as $\Lambda = d_1 + d_2 = 1000$ nm, $w_1 + w_2 = 300$ nm, metal thickness $h = 50$ nm, and film thickness $t = 500$ nm. (b), (c) Mode profiles of the optical resonances excited by normal-incident x-polarized plane waves. The color indicates the amplitude of the electric field, while the gray arrows indicate the direction of the electric field.

grating either nonequal distance ($d_1 \neq d_2$) or nonequal width ($w_1 \neq w_2$). (Similar one-dimensional metallic or dielectric gratings can be found in the literature [28–30]). The period of the modified one-dimensional system is truly Λ. As an example, Fig. 2(b) shows the band diagram for $|d_1 - d_2|/2 = 50$ nm, and now the target modes are shifted to the center of the irreducible Brillouin zone. Figure 3(a) further shows the transmission spectra under the excitation of a normal-incident x-polarized plane wave, and there is an asymmetric dip for

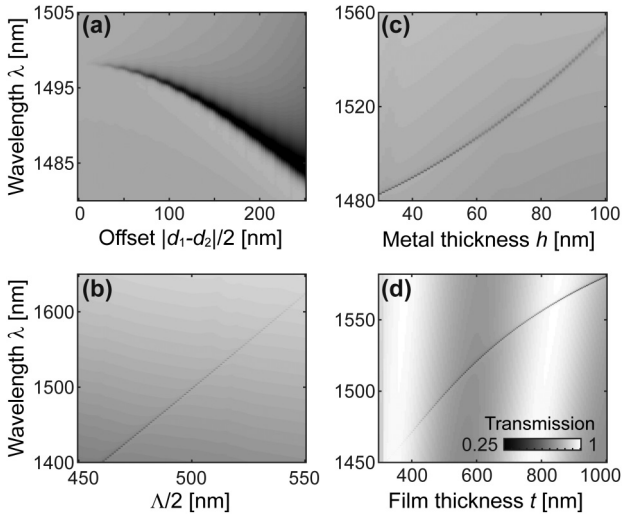

FIG. 4. Dependence of the resonance wavelength for the mode induced by nonequal distance in metal strips, on (a) the offset $|d_1 - d_2|/2$, (b) the period Λ, (c) the metal thickness h, and (d) the film thickness t.

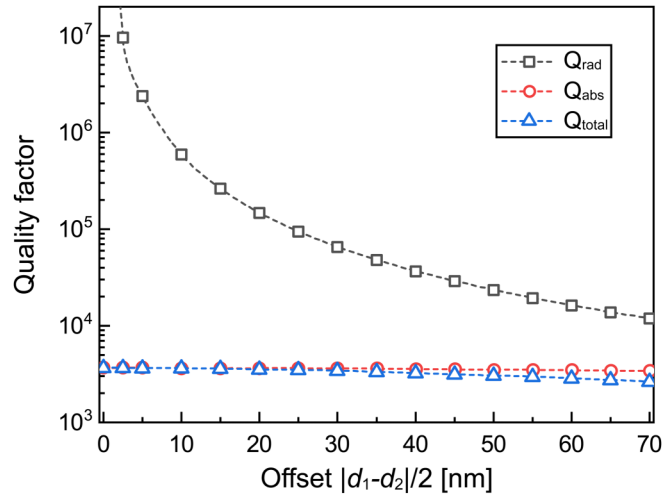

FIG. 5. Quality factors (Q_{total}, Q_{rad}, and Q_{abs}) as a function of the offset ($|d_1 - d_2|/2$). Other parameters are $\Lambda = 1000$ nm, $w_1 = w_2 = 150$ nm, $h = 50$ nm, and $t = 500$ nm.

either $d_1 \neq d_2$ or $w_1 \neq w_2$ (to be more specific, $|d_1 - d_2|/2 = 50$ nm, or $|w_1 - w_2|/2 = 50$ nm). When an open system is externally illuminated, the presence of highly confined modes is often manifested as narrow asymmetric resonances. By checking the field distributions at the transmission dips, we found that the resonance mode labeled as M1 [Fig. 3(b); $d_1 \neq d_2$] resembles the eigenmode in Fig. 1(c), while M2 [Fig. 3(c); $w_1 \neq w_2$] resembles the eigenmode in Fig. 1(d). Note that only one of these two resonances can be excited at normal incidence, while the other one remains dark if only one parameter is modified (either $d_1 \neq d_2$ or $w_1 \neq w_2$). In the following discussion we focus on gratings with metal strips of nonequal distance ($d_1 \neq d_2$), because inside the polymer layer the distribution of the induced optical mode in Fig. 1(c) matches with the distribution of the electrostatic field in Fig. 1(b), and the latter governs the orientation and amplitude of r_{33}. Figure 4 shows the dependence of the resonance wavelength of this mode on each individual structure parameter. With increasing offset between d_1 and d_2, the resonance wavelength becomes shorter [Fig. 4(a)]. The resonance wavelength can be shifted to a longer side by increasing the period Λ, the metal thickness h, or the film thickness t [Figs. 4(b)–4(d)]. The linewidth also increases with increasing thickness of the metal [Fig. 4(c)]. Therefore, this resonance can be easily tuned to, for example, the typical optical communication wavelength around 1550 nm.

As shown in Fig. 4(a), the linewidth decreases with decreasing offset between d_1 and d_2. Due to the presence of dissipative losses, this system does not exhibit resonances with a diverging Q factor. However, the radiative quality factor (Q_{rad}) can be diverging (Fig. 5). Here Q_{rad} was calculated by assuming pure real permittivity for the metal and EO polymer, and the material absorption-related quality factor Q_{abs} was obtained by the relation $1/Q_{\text{abs}} = 1/Q_{\text{total}} - 1/Q_{\text{rad}}$. When decreasing the offset $|d_1 - d_2|/2$, all these factors (Q_{total}, Q_{rad}, and Q_{abs}) increase, as the supported leaky mode is finally decoupled from free-space radiation, resulting in a bound state and thus a diverging Q_{rad}. The main energy dissipation occurs on the lateral surfaces of the metal strips. With increasing offset $|d_1 - d_2|/2$, the field distribution gets distorted and the dissipation on the top surface of the metal strips increases, leading to a decreasing Q_{abs} (from $Q_{\text{abs}} = 3600$ at $d_1 = d_2$ to $Q_{\text{abs}} = 3400$ at $|d_1 - d_2|/2 = 70$ nm). Q_{total} decreases much faster, from $Q_{\text{total}} = 3600$ at $d_1 = d_2$ to $Q_{\text{total}} = 3000$ at $|d_1 - d_2|/2 = 50$ nm, due to increased radiative losses.

By applying an external voltage to the electrodes after poling, an electrostatic field is formed inside the EO polymer layer, which changes the refractive index of this layer via the linear Pockels effect. The poled polymer is anisotropic and the nonlinear susceptibility is a tensor. Furthermore, as a result of the spatially varying magnitude and orientation of the poling field, the dominant element of the linear Pockels EO effect tensor r_{33} and the refractive index change Δn also vary spatially [16]. Therefore, a rigorous analysis would be very difficult. Instead, we show in Fig. 6 the simulated shifting of the resonance by assuming a homogeneous and isotropic change in the refractive index of the EO polymer layer from $\Delta n = -0.005$ to 0.005 with a step of 0.001. Therefore, an index change of $\Delta n = 0.00125$ can fully shift the resonance away from its unbiased position. Based on the relation $\Delta n = -0.5 n_0^3 r_{33} V_0/d$, where n_0 is the refractive index of the EO polymer at zero bias and d is the distance between the electrodes, we estimate that the required driving voltage V_0 can be well below 10 V, by assuming $r_{33} = 100$ pm/V and $d = 0.5\ \mu$m.

At this moment, one may like to have a comparison with the regular case, namely, the one-dimensional grating with only one metal strip within one period of Λ (similar to that utilized in Ref. [16]). To bring the resonances around $\lambda = 1500$ nm for comparison, the thickness of the EO polymer layer is set to be $t = 600$ nm, and the width of the metal strip is set to be $w = 200$ nm, while other parameters are kept the same as before. Figure 7(a) shows the dispersion, obtained by stitching together the zeroth-order transmission as a function of incident angle ranging from 0° to 5° under

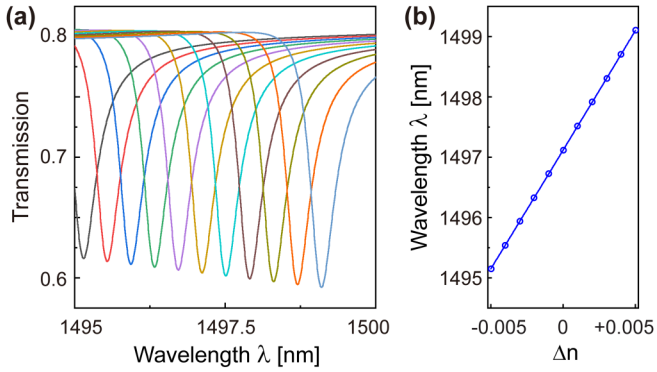

FIG. 6. Shifting the resonance by variation in the refractive index of the EO polymer layer. (a) Transmission spectra with a homogeneous and isotropic index change from $\Delta n = -0.005$ to 0.005 with a step of 0.001. Other parameters are $\Lambda = 1000$ nm, $|d_1 - d_2|/2 = 50$ nm, $w_1 = w_2 = 150$ nm, $h = 50$ nm, and $t = 500$ nm. (b) Resonance wavelength at the transmission dip as a function of Δn. The solid line is a linear fit.

TM polarization. The profiles of the band-edge modes at the Γ point, shown in Fig. 7(b), closely resemble those in Fig. 2. The upper band-edge mode is antisymmetric and thus cannot be excited at normal incidence, whereas the lower band-edge mode is symmetric. The quality factor of the antisymmetric mode ($Q_{\text{total}} = 5100$) is higher than those in Fig. 2 because of the lesser amount of metal here. In contrast, the symmetric mode shows a much lower quality factor ($Q_{\text{total}} = 340$). For the same amount of change in Δn, the shift in wavelength in Fig. 7(c) is slightly larger than that in Fig. 6, implying that this symmetric mode can be utilized in scenarios where a large tuning of broad resonances is preferred instead of a complete shift of the resonances. However, because of the

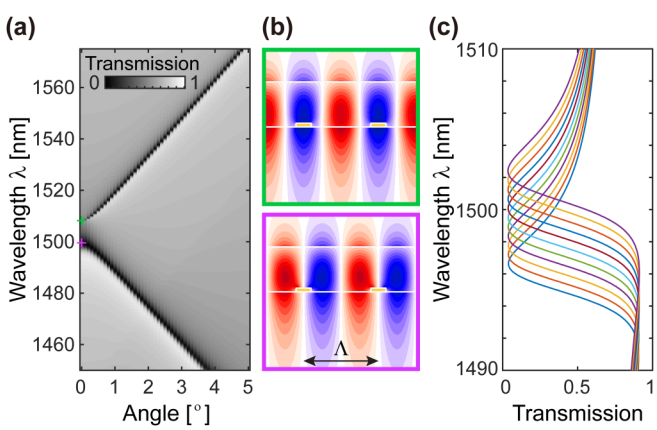

FIG. 7. One-dimensional grating with only one metal strip in one period of Λ. (a) Angle-resolved transmission spectra showing the dispersion. The parameters are $\Lambda = 1000$ nm, $w = 200$ nm, $h = 50$ nm, and $t = 600$ nm. (b) Mode profiles of the E_z component at the Γ-point band edges. The upper band-edge mode is antisymmetric and thus cannot be excited at normal incidence, while the lower band-edge mode is symmetric. (c) Transmission spectra with a homogeneous and isotropic index change in the EO polymer layer, from $\Delta n = -0.005$ to 0.005 with a step of 0.001.

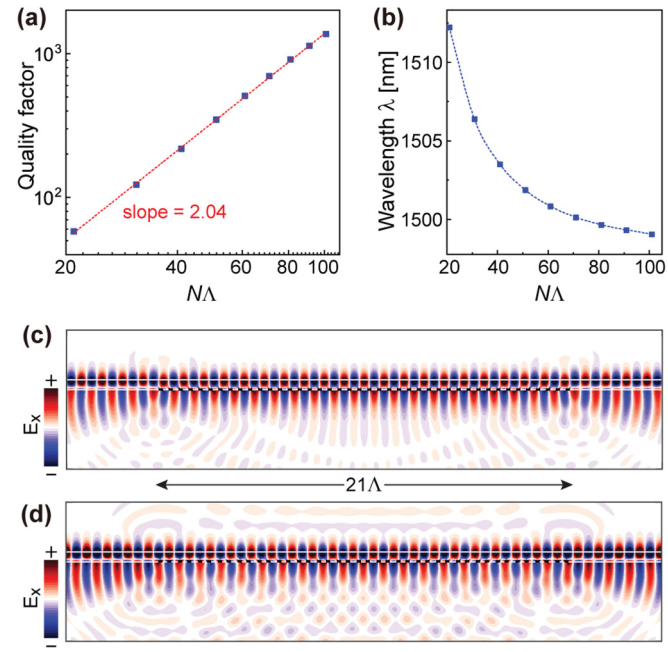

FIG. 8. Resonances in finite slabs with different lateral size along the x direction. (a), (b) Q_{total} and the resonance wavelength as a function of the lateral size $N\Lambda$, ranging from 21Λ to 101Λ. The dashed line is the linear fit indicating that Q_{total} grows quadratically with N in this size range. (c), (d) Mode profile of the E_z component for the 21Λ finite slab with $d_1 = d_2$ and $|d_1 - d_2|/2 = 50$ nm, respectively. Other parameters are $\Lambda = 1000$ nm, $w_1 = w_2 = 150$ nm, $h = 50$ nm, and $t = 500$ nm.

doubled distance between the electrodes, the required driving voltage would be much larger.

All the discussion above is based on infinite arrays. In practice, we deal with a finite lateral size, $N\Lambda$, especially when making the array as a pixel. Figure 8(a) shows the quality factor Q_{total} as a function of lateral size along the x direction ranging from 21Λ to 101Λ. This plot was obtained from eigenfrequency calculations with $d_1 = d_2$, but a similar trend holds for $d_1 \neq d_2$ because for the latter Q_{total} does not differ too much. In this size range Q_{total} grows quadratically with N (similar to the symmetry-protected BIC mode [31,32]). Of course, Q_{total} would finally saturate with increasing lateral size due to the limitation from the dissipative losses. For a small lateral size, the resonance wavelengths are different in the finite and infinite slabs, but approach that of the infinite slab quickly [Fig. 8(b)]. As shown in Fig. 8(c), energy leaks mainly from the truncated sides of the slab when $d_1 = d_2$. For $d_1 \neq d_2$ [Fig. 8(d)], there exists additional leakage along the vertical direction, to allow coupling with external radiation.

III. EXPERIMENTAL VERIFICATION USING SILVER GRATING AND ALUMINA SLAB WAVEGUIDE

The EO polymer is not commercially available. Here we experimentally verify the phenomena in Fig. 3(a), using alumina to mimic the EO polymer because alumina has a refractive index close to the EO polymer mentioned above. For the material of the grating, we chose a less expensive metal, silver. Therefore, both the metal grating and the core

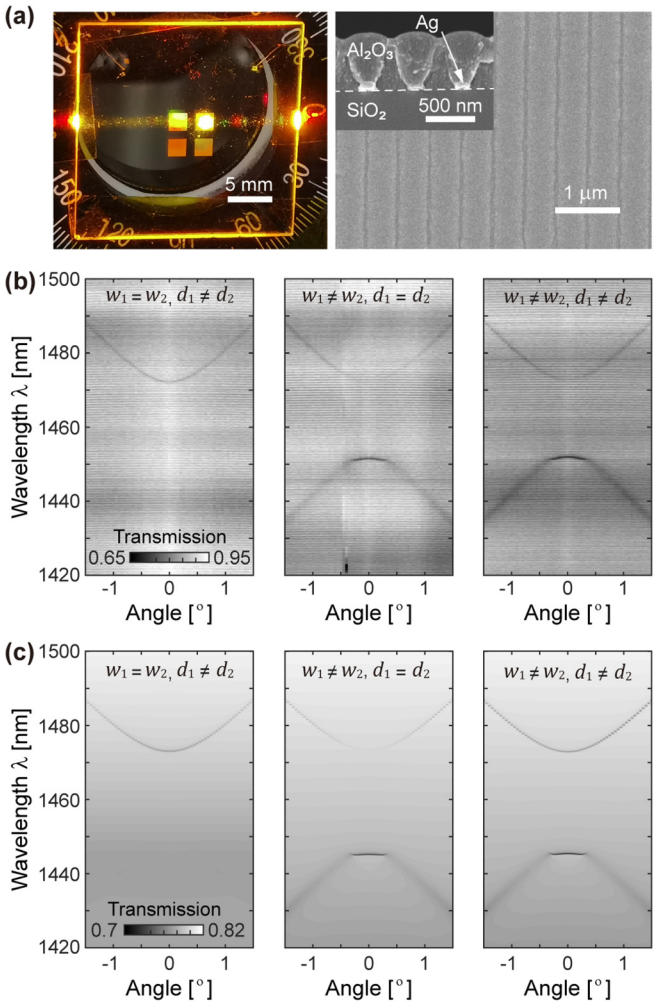

FIG. 9. Experimental verification with silver grating and alumina slab waveguide. (a) Photograph and SEM images of the sample. (b) Measured transmission spectra for ($w_1 = w_2$, $|d_1 - d_2| = 50$ nm), ($|w_1 - w_2| = 50$ nm, $d_1 = d_2$), and ($|w_1 - w_2| = 50$ nm, $|d_1 - d_2| = 50$ nm). (c) Simulated transmission spectra based on parameters from SEM images and ellipsometry fitting.

of the waveguide had much lower dissipative losses than those in the theoretical model of the previous section, and ideally, we could expect a much higher Q. We fabricated three arrays with ($w_1 = w_2$, $|d_1 - d_2| = 50$ nm), ($|w_1 - w_2| = 50$ nm, $d_1 = d_2$), and ($|w_1 - w_2| = 50$ nm, $|d_1 - d_2| = 50$ nm) on a quartz substrate of 1 mm thickness, together with one array with ($w_1 = w_2$ and $d_1 = d_2$) for reference, using electron-beam lithography and subsequently electron-beam evaporation. Other nominal structure parameters were the same as in Fig. 3. Each array had a size of 2 mm × 2 mm, in order to be measurable in free space with a collimated light beam as shown in Fig. 9(a). The arrays were illuminated with a collimated beam from a supercontinuum source (SuperK COMPACT, NKT Photonics), and the zeroth-order transmission was coupled into a multimode fiber and delivered to an optical spectrum analyzer (AQ6370D, Yokogawa). The spectra were normalized to the transmission through the empty area of the same sample.

Due to the presence of the Fabry-Pérot interference related to the quartz substrate, it was very difficult to discriminate the target high-Q resonances from the normal-incident transmission spectra. Instead, the transmission spectra as a function of the incident angle were stitched together to help identify the resonances, as shown in Fig. 9(b). Over the background of the Fabry-Pérot ripples, the transmission minima (dark color) as a function of the incident angle indicated the dispersion bands of the resonances supported by this hybrid structure. For comparison, the simulated angle-resolved transmission spectra were shown in Fig. 9(c), calculated based on parameters from SEM images and ellipsometry fitting. From the cross-sectional and top-view SEM images [Fig. 9(a)], we found that the top surface of the arrays was not flat, as a result of sequential deposition of the silver grating and the alumina layer. However, simulation confirmed that this periodically corrugated surface did not change the spectra obviously compared to a flat top surface. Overall, the measurement was in good agreement with the simulation (the deviation in wavelengths can be attributed to the imperfection in the fabrication), and both showed the same trend as in Fig. 3(a). At normal incidence, a transmission dip appeared at the longer-wavelength side for ($w_1 = w_2$ and $d_1 \neq d_2$), while for ($w_1 \neq w_2$ and $d_1 = d_2$) a transmission dip appeared at the shorter-wavelength side. For these two cases, the other dip did not show up at normal incidence because of the symmetry mismatch. With both changes together ($w_1 \neq w_2$ and $d_1 \neq d_2$), both dips appeared. From the linewidth of the transmission dips, we estimated that the measured Q was well above 1000.

IV. CONCLUSIONS

In summary, we have presented a method to engineer the quasibound state in a slab waveguide with an EO polymer as the core, in order to reduce the required voltage to fully shift the optical resonance for modulation. By slightly changing the relative position of the neighboring metal strips constituting the grating, the guided mode with the same periodicity as the electrostatic field can be made accessible from free space with controllable radiation damping. The width of the metal strips can be further utilized to engineer the phase change for steering the diffracted beam. This method also offers prospects for engineering narrow-linewidth resonances from metallic or dielectric gratings for other applications.

ACKNOWLEDGMENTS

This work was partially supported by the National Natural Science Foundation of China (Grants No. 12074227, No. 12192254, No. 91750201, and No. 11974218), National Key Research and Development Project of China (Grant No. 2019YFA0705000), Innovation Group of Jinan (Grant No. 2018GXRC010), Local Science and Technology Development Project of the Central Government (Grant No. YDZX20203700001766), and Natural Science Foundation of Guangdong Province (Grants No. 2018A0303130056 and No. 2020A1515010491).

[1] A. M. Shaltout, V. M. Shalaev, and M. L. Brongersma, Spatiotemporal light control with active metasurfaces, Science **364**, eaat3100 (2019).

[2] A. Smolyaninov, A. El Amili, F. Vallini, S. Pappert, and Y. Fainman, Programmable plasmonic phase modulation of free-space wavefronts at gigahertz rates, Nat. Photonics **13**, 431 (2019).

[3] Y.-W. Huang, H. W. H. Lee, R. Sokhoyan, R. A. Pala, K. Thyagarajan, S. Han, D. P. Tsai, and H. A. Atwater, Gate-tunable conducting oxide metasurfaces, Nano Lett. **16**, 5319 (2016).

[4] G. Kafaie Shirmanesh, R. Sokhoyan, R. A. Pala, and H. A. Atwater, Dual-gated active metasurface at 1550 nm with wide (>300°) phase tunability, Nano Lett. **18**, 2957 (2018).

[5] G. K. Shirmanesh, R. Sokhoyan, P. C. Wu, and H. A. Atwater, Electro-optically tunable multifunctional metasurfaces, ACS Nano **14**, 6912 (2020).

[6] J. Park, B. G. Jeong, S. I. Kim, D. Lee, J. Kim, C. Shin, C. B. Lee, T. Otsuka, J. Kyoung, S. Kim, K. Y. Yang, Y. Y. Park, J. Lee, I. Hwang, J. Jang, S. H. Song, M. L. Brongersma, K. Ha, S. W. Hwang, H. Choo *et al.*, All-solid-state spatial light modulator with independent phase and amplitude control for three-dimensional LiDAR applications, Nat. Nanotechnol. **16**, 69 (2021).

[7] P. C. Wu, R. A. Pala, G. Kafaie Shirmanesh, W. H. Cheng, R. Sokhoyan, M. Grajower, M. Z. Alam, D. Lee, and H. A. Atwater, Dynamic beam steering with all-dielectric electro-optic III-V multiple-quantum-well metasurfaces, Nat. Commun. **10**, 3654 (2019).

[8] C. Haffner, W. Heni, Y. Fedoryshyn, J. Niegemann, A. Melikyan, D. L. Elder, B. Baeuerle, Y. Salamin, A. Josten, U. Koch, C. Hoessbacher, F. Ducry, L. Juchli, A. Emboras, D. Hillerkuss, M. Kohl, L. R. Dalton, C. Hafner, and J. Leuthold, All-plasmonic Mach-Zehnder modulator enabling optical high-speed communication at the microscale, Nat. Photonics **9**, 525 (2015).

[9] C. Wang, M. Zhang, X. Chen, M. Bertrand, A. Shams-Ansari, S. Chandrasekhar, P. Winzer, and M. Loncar, Integrated lithium niobate electro-optic modulators operating at CMOS-compatible voltages, Nature (London) **562**, 101 (2018).

[10] H. Xu, F. Liu, D. L. Elder, L. E. Johnson, Y. de Coene, K. Clays, B. H. Robinson, and L. R. Dalton, Ultrahigh electro-optic coefficients, high index of refraction, and long-term stability from Diels-Alder cross-linkable binary molecular glasses, Chem. Mater. **32**, 1408 (2020).

[11] F. Ren III, M. Li, Q. Gao, W. Cowell, J. Luo, A. K. Y. Jen, and A. X. Wang, Surface-normal plasmonic modulator using sub-wavelength metal grating on electro-optic polymer thin film, Opt. Commun. **352**, 116 (2015).

[12] J. Zhang, Y. Kosugi, A. Otomo, Y.-L. Ho, J.-J. Delaunay, Y. Nakano, and T. Tanemura, Electrical tuning of metal-insulator-metal metasurface with electro-optic polymer, Appl. Phys. Lett. **113**, 231102 (2018).

[13] X. Sun, H. Yu, N. Deng, D. Ban, G. Liu, and F. Qiu, Electro-optic polymer and silicon nitride hybrid spatial light modulators based on a metasurface, Opt. Express **29**, 25543 (2021).

[14] J. Zhang, Y. Kosugi, A. Otomo, Y. Nakano, and T. Tanemura, Active metasurface modulator with electro-optic polymer using bimodal plasmonic resonance, Opt. Express **25**, 30304 (2017).

[15] A. Feng, Z. Yu, and X. Sun, Ultranarrow-band metagrating absorbers for sensing and modulation, Opt. Express **26**, 28197 (2018).

[16] I. C. Benea-Chelmus, M. L. Meretska, D. L. Elder, M. Tamagnone, L. R. Dalton, and F. Capasso, Electro-optic spatial light modulator from an engineered organic layer, Nat. Commun. **12**, 5928 (2021).

[17] S. Fan and J. D. Joannopoulos, Analysis of guided resonances in photonic crystal slabs, Phys. Rev. B **65**, 235112 (2002).

[18] A. Christ, S. G. Tikhodeev, N. A. Gippius, J. Kuhl, and H. Giessen, Waveguide-Plasmon Polaritons: Strong Coupling of Photonic and Electronic Resonances in a Metallic Photonic Crystal Slab, Phys. Rev. Lett. **91**, 183901 (2003).

[19] S. G. Tikhodeev, N. A. Gippius, A. Christ, T. Zentgraf, J. Kuhl, and H. Giessen, Waveguide-plasmon polaritons in photonic crystal slabs with metal nanowires, Phys. Status Solidi (c) **2**, 795 (2005).

[20] R. Kikkawa, M. Nishida, and Y. Kadoya, Bound states in the continuum and exceptional points in dielectric waveguide equipped with a metal grating, New J. Phys. **22**, 073029 (2020).

[21] S. I. Azzam, V. M. Shalaev, A. Boltasseva, and A. V. Kildishev, Formation of Bound States in the Continuum in Hybrid Plasmonic-Photonic Systems, Phys. Rev. Lett. **121**, 253901 (2018).

[22] F. Monticone and A. Alù, Bound states within the radiation continuum in diffraction gratings and the role of leaky modes, New J. Phys. **19**, 093011 (2017).

[23] I.-C. Benea-Chelmus, S. Mason, M. L. Meretska, D. L. Elder, D. Kazakov, A. Shams-Ansari, L. R. Dalton, and F. Capasso, Gigahertz free-space electro-optic modulators based on Mie resonances, Nat. Commun. **13**, 3170 (2022).

[24] S. P. Palto, M. I. Barnik, V. V. Artemov, N. M. Shtykov, A. R. Geivandov, S. G. Yudin, and M. V. Gorkunov, Liquid crystal on subwavelength metal gratings, J. Appl. Phys. **117**, 223108 (2015).

[25] M. V. Gorkunov, I. V. Kasyanova, V. V. Artemov, M. I. Barnik, A. R. Geivandov, and S. P. Palto, Fast Surface-Plasmon-Mediated Electro-Optics of a Liquid Crystal on a Metal Grating, Phys. Rev. Appl. **8**, 054051 (2017).

[26] P. B. Johnson and R. W. Christy, Optical constants of the noble metals, Phys. Rev. B **6**, 4370 (1972).

[27] S. G. Johnson, S. Fan, P. R. Villeneuve, J. D. Joannopoulos, and L. A. Kolodziejski, Guided modes in photonic crystal slabs, Phys. Rev. B **60**, 5751 (1999).

[28] O. V. Borovkova, H. Hashim, D. O. Ignatyeva, M. A. Kozhaev, A. N. Kalish, S. A. Dagesyan, A. N. Shaposhnikov, V. N. Berzhansky, V. G. Achanta, L. V. Panina, A. K. Zvezdin, and V. I. Belotelov, Magnetoplasmonic structures with broken spatial symmetry for light control at normal incidence, Phys. Rev. B **102**, 081405(R) (2020).

[29] F. Wu, M. Luo, J. Wu, C. Fan, X. Qi, Y. Jian, D. Liu, S. Xiao, G. Chen, H. Jiang, Y. Sun, and H. Chen, Dual quasibound states in the continuum in compound grating waveguide structures for large positive and negative Goos-Hänchen shifts with perfect reflection, Phys. Rev. A **104**, 023518 (2021).

[30] A. I. Ovcharenko, C. Blanchard, J.-P. Hugonin, and C. Sauvan, Bound states in the continuum in symmetric and

asymmetric photonic crystal slabs, Phys. Rev. B **101**, 155303 (2020).

[31] E. N. Bulgakov and A. F. Sadreev, High-Q resonant modes in a finite array of dielectric particles, Phys. Rev. A **99**, 033851 (2019).

[32] Z. F. Sadrieva, M. A. Belyakov, M. A. Balezin, P. V. Kapitanova, E. A. Nenasheva, A. F. Sadreev, and A. A. Bogdanov, Experimental observation of a symmetry-protected bound state in the continuum in a chain of dielectric disks, Phys. Rev. A **99**, 053804 (2019).